RSC Advances

PAPER

View Article Online
View Journal | View Issue

Cite this: *RSC Adv.*, 2021, **11**, 2706

A novel red-emitting phosphor $Mg_2Y_2Al_2Si_2O_{12}:Ce^{3+}/Mn^{2+}$ for blue chip-based white LEDs

Zhipeng Wang,[a] Zhijun Wang,*[a] Yuebin Li,[a] Jinjin Liu,[a] Qi Bao,[a] Xiangyu Meng,[a] Keliang Qiu,[a] Zhiping Yang,[a] Dawei Wang*[b] and Panlai Li*[a]

Traditional white light-emitting diodes (LEDs) (blue chip + YAG:Ce^{3+} yellow phosphor) have the limitation of red deficiency, which limits their application in the illumination field. The single cation/anion substitution or co-doping of activators can increase the red component; however, the large energy loss is attributed to the ultra-long Stokes shift and energy transfer. This work attempts to utilize the short-distance Stokes shift and a small amount of energy transfer to increase the red component in two steps. First, based on a large number of previous research results, the $Mg_2Y_2Al_2Si_2O_{12}:Ce^{3+}$ phosphor is selected. Second, additional enhancement of the red component in the emission spectrum was achieved by ion co-doping Mn^{2+} into $Mg_2Y_2Al_2Si_2O_{12}:Ce^{3+}$. The emission peaks for samples $Mg_2Y_2Al_2Si_2O_{12}:Ce^{3+},Mn^{2+}$ shift from 600 to 635 nm with increase in the concentration of Mn^{2+}, and the emission spectra intensity of $Mg_{1.97}Y_{1.93}Al_2Si_2O_{12}$:0.07 Ce^{3+},0.03 Mn^{2+} anomalously increased by ~37%, which was attributed to the increase in the distance between Ce^{3+} ions because of the doping of Mn^{2+} ions, and reduction in the concentration of defects in the crystal, resulting in the energy loss decreases of Ce^{3+}. The emission peak of $Mg_{1.97}Y_{1.93}Al_2Si_2O_{12}$:0.07 Ce^{3+},0.03 Mn^{2+} shifts to 618 nm and the quantum efficiency was as high as 83.07%. Furthermore, this sample has high thermal stability and the emission intensity was still 80.14% at 120 °C. As such, it has great potential in the application of white LEDs.

Received 1st November 2020
Accepted 7th December 2020

DOI: 10.1039/d0ra09289d

rsc.li/rsc-advances

1 Introduction

Traditional white LEDs (the blue-chip + YAG:Ce^{3+} yellow phosphor) have superior properties of high brightness and low cost and are extensively used in transportation, lighting displays, medical devices, electronic products and other fields. However, because of the lack of red-light components, color rendering and color temperature of white LEDs is insufficient to meet the increasing lighting requirements. For example, in the field of high-color restored lighting or warm white lighting, it cannot compete with other white lighting solutions.[1–6] In general, the red light component of the phosphor can be increased by co-doping other activating ions, *e.g.*, Jia *et al.* reported the YAG:Ce^{3+},Mn^{2+} phosphor with the two emission peaks at 540 nm (Ce^{3+}) and 594 nm (Mn^{2+}), which increases the red component of the emission with increasing Mn^{2+} concentration.[7] However, adding sufficient red components requires Ce^{3+} to transfer a large amount of energy to enhance the emission intensity of Mn^{2+} ions.[8–11] However, it causes a large amount of energy loss, which reduces the overall luminous intensity of the phosphor. Furthermore, the substitution of anions/cations to adjust the crystal field environment of Ce^{3+} ions can regulate the emission spectrum of Ce^{3+} ions to the long-wave direction and increase the red component. A large number of researchers have adjusted the emission spectrum of YAG:Ce^{3+} by this method and obtained a large number of results to achieve the movement of the emission peak from 532 to 622 nm.[12–14] However, with the redshift of the emission spectrum, its Stokes shift increases, the quenching effect increases, and the emission intensity of the phosphor gradually decreases, which limits the application of the phosphor. The energy loss caused by the ultra-long Stokes shift and a large amount of energy transfer is extremely large. Either method cannot obtain high-efficiency phosphors alone; this work attempts to combine two methods to prepare a highly efficient red phosphor in two steps. Firstly, initially improve the red component of Ce^{3+} ion emission spectrum using structural fine-tuning, while ensuring that the phosphor has relatively strong luminescence intensity. Pan *et al.* reported an orange (600 nm) emitting phosphor $Mg_2Y_2Al_2Si_2O_{12}:Ce^{3+}$ with quantum efficiency as high as 58.3%;[15] as such, the $Mg_2Y_2Al_2Si_2O_{12}:Ce^{3+}$ phosphor is selected based on a large number of previous research results. Second, additional enhancement in the red component of the emission spectrum

[a]*National-Local Joint Engineering Laboratory of New Energy Photoelectric Devices, Hebei Key Laboratory of Optic-electronic Information and Materials, College of Physics Science & Technology, Hebei University, Baoding 071002, China. E-mail: wangzj1998@126.com; li_panlai@126.com*

[b]*Hebei Key Laboratory of Semiconductor Lighting and Display Critical Materials, Baoding, 071000, China. E-mail: D.Wang@ledphor.com*

by co-doping Mn^{2+} with $Mg_2Y_2Al_2Si_2O_{12}$:Ce^{3+}; moreover, it is desired to obtain a highly efficient red phosphor. Finally, when the doping concentration of Mn^{2+} is 0.03, the emission peak of $Mg_2Y_2Al_2Si_2O_{12}$:Ce^{3+},Mn^{2+} shifts to 618 nm, and the quantum efficiency is as high as 83.07%. Furthermore, the emission intensity of the sample $Mg_{1.97}Y_{1.93}Al_2Si_2O_{12}$:0.07 Ce^{3+},0.03 Mn^{2+} is still 80.14% at 120 °C, indicating that this sample has a higher thermal stability. By mixing this sample with YAG:Ce^{3+}, a warm white light with a high color index of 78 and abundant red light components is obtained, stimulated by the 460 nm-sized blue chip. It has great potential in applying white LEDs.

2 Sample preparation and characterization

A series of $Mg_2Y_2Al_2Si_2O_{12}$, $Mg_{2-y}Y_{1.93}Al_2Si_2O_{12}$:0.07 Ce^{3+},yMn^{2+}(y = 0, 0.01, 0.02, 0.03, 0.04, 0.06, 0.08, 0.12, 0.16) and $Mg_{1.97}Y_{2-x}Al_2Si_2O_{12}$:$xCe^{3+}$,0.03 Mn^{2+} (x = 0, 0.001, 0.005, 0.01, 0.03, 0.05, 0.07) samples were synthesized by a high temperature solid-state method. The raw materials were MgO (A.R.), Y_2O_3 (99.999%), Al_2O_3 (A.R.), SiO_2 (A.R.), CeO_2 (99.999%), and $MnCO_3$ (A.R.). Firstly, the raw materials were weighed as per the stoichiometric ratio, and then they were placed in an agate mortar and ground for 20 min; the ground powders were placed in a corundum, and then placed in a box furnace for sintering by heating to 1650 °C and held for 5 h. Finally, the samples were naturally cooled to room temperature, and the samples were taken out and placed in an agate mortar for grinding to obtain powder samples for the subsequent measurements.

2.1 Phase structure characterization

The phase structures of the samples were characterized using a Bruker D8 X-ray diffractometer. The radiation source was Cu target K_α (λ = 0.15406 nm), and the working voltage and current were 40 kV and 40 mA, respectively. The scan range 2θ and the step size were 10–80° and 0.02° s^{-1}, respectively.

2.2 Optical properties

The steady-state spectra of the samples were measured using a Hitachi F-4600 fluorescence spectrometer. The sample thermoluminescence spectra (TL) were measured using an FJ-427A1 type thermoluminescence meter, and the measurement range and heating rate were 50–300 °C and 1 °C s^{-1}, respectively. The samples were irradiated for 5 min under UV light and then placed in a dark room for 10 min before thermoluminescence measurements were taken.

2.3 Fluorescence lifetime and quantum efficiency

The lifetimes of samples were monitored using a Horiba FL3 instrument. The lifetime of Ce^{3+} was achieved using 320 and 455 nm nano-LEDs as exciting sources, and the lifetime of Mn^{2+} was measured using a Xe lamp as the light source. The quantum efficiencies of samples were measured using the Hitachi F-7000 fluorescence spectrophotometer and a Hitachi 5J0-0148 integrating sphere.

3 Results and discussion

3.1 XRD pattern and crystal structure

Fig. 1(a) shows the unit cell of $Mg_2Y_2Al_2Si_2O_{12}$. There are three different lattice positions in the stability of the garnet structure. The Y/Mg atom has eight coordination oxygen atoms together to form a dodecahedron with two different bond lengths. The length

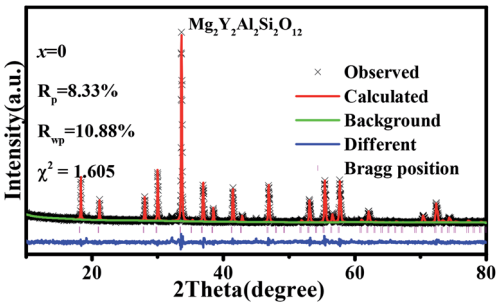

Fig. 2 XRD refinement of $Mg_2Y_2Al_2Si_2O_{12}$.

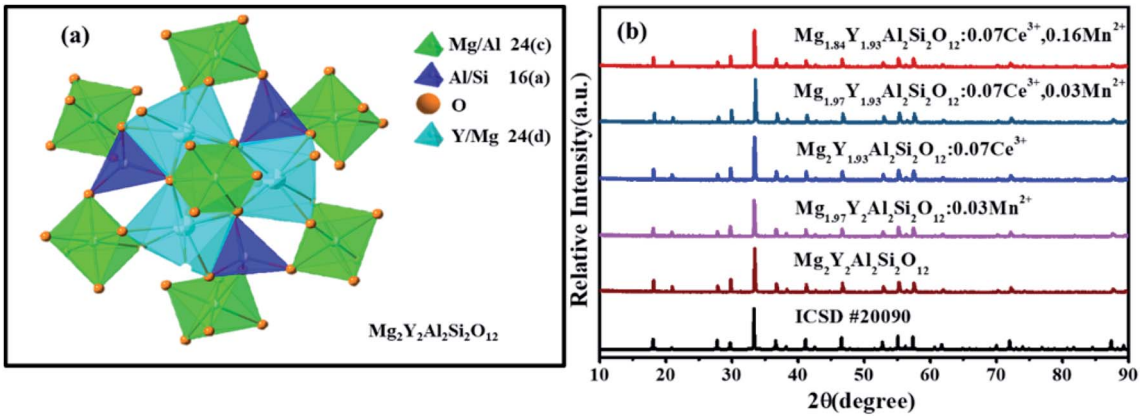

Fig. 1 (a) The unit cell of $Mg_2Y_2Al_2Si_2O_{12}$. (b) XRD patterns of $Mg_2Y_2Al_2Si_2O_{12}$, $Mg_{1.97}Y_2Al_2Si_2O_{12}$:0.03 Mn^{2+}, $Mg_2Y_{1.93}Al_2Si_2O_{12}$:0.07 Ce^{3+}, $Mg_{1.97}Y_{1.93}Al_2Si_2O_{12}$:0.07 Ce^{3+},0.03 Mn^{2+}, $Mg_{1.84}Y_{1.93}Al_2Si_2O_{12}$:0.07 Ce^{3+},0.16 Mn^{2+}.

of the four shorter keys is m and the length of four longer keys is n. The Y/Mg atom occupies 24(c) sites in the unit cell. The Mg/Al atom has six coordination oxygen atoms together to form an octahedron, which has the same bond length p and occupies 16(a) sites in the unit cell. The Al/Si atom occupies the 24(d) site and has four coordinating oxygen atoms to form a tetrahedron, which has the same bond length q. Fig. 1(b) shows the XRD patterns of representative samples $Mg_2Y_2Al_2Si_2O_{12}$, $Mg_{1.97}Y_2Al_2Si_2O_{12}$:0.03 Mn^{2+}, $Mg_2Y_{1.93}Al_2Si_2O_{12}$:0.07 Ce^{3+}, $Mg_{1.97}Y_{1.93}Al_2Si_2O_{12}$:0.07 Ce^{3+},0.03 Mn^{2+} and $Mg_{1.84}Y_{1.93}Al_2Si_2O_{12}$:0.07 Ce^{3+},0.16 Mn^{2+}. The XRD diffraction peak positions of the synthetic samples match well with the diffraction peak in the standard card $Y_3Al_5O_{12}$ (ICSD#20090), indicating that all the samples have a single-crystal phase and that the Ce^{3+} and Mn^{2+} ions do not destroy the crystal structure. The XRD patterns of samples are subjected to refinement using the standard card $Y_3Al_5O_{12}$ (ICSD#20090) as a standard, and the obtained refinement data are within the accurate range and are shown in Fig. 2–4.

3.2 Luminescence properties of $Mg_2Y_{1.93}Al_2Si_2O_{12}$:0.07 Ce^{3+} and $Mg_{1.97}Y_2Al_2Si_2O_{12}$:0.03 Mn^{2+}

Fig. 5(a) and (b) show the excitation spectra and emission spectra of $Mg_2Y_{1.93}Al_2Si_2O_{12}$:0.07 Ce^{3+} two luminescence centers. The luminescence centers come from the Ce^{3+} ions substituting Y^{3+} ions to occupy eight coordination sites.[15] The emission spectra of Ce^{3+}in fluorides and oxides can generally move from the ultraviolet region to the blue region. However, in the environment of strong covalent and crystal field, the 5d energy level of Ce^{3+} ions can move to a lower energy range; therefore, Ce^{3+} can emit yellow or even red fluorescence color.[7,8,16] In the study of sulfides and nitrides, the 5d energy levels of Ce^{3+}ions can be divided into two to five energy levels, and the number of separations depend on the symmetry of the lattice containing Ce^{3+}ligands. In the cubic symmetry crystal structure, such as garnet structure, the 5d state is split into two energy levels (e_g and t_g^2), and the crystal field can be split further in the twisted cubic crystal.[17–22] The unique longwave emission (green yellow-orange) of Ce^{3+} in the garnet is attributed to the splitting of the crystal field of the energy level eg into a lower $5d_1$ level and a higher energy $5d_2$ level with an interval of about 8000 cm^{-1}. It is precise because of this energy level splitting the emission from the highest energy $5d_2$ level is in the blue-violet spectral region; the emission from the lowest energy $5d_1$ level is in the green yellow-orange spectral region.[23–27] It is seen from Fig. 5(a), under the excitation of 332 nm, the emission spectrum of Ce^{3+} extends from 350 to 700 nm, and the emission peak is

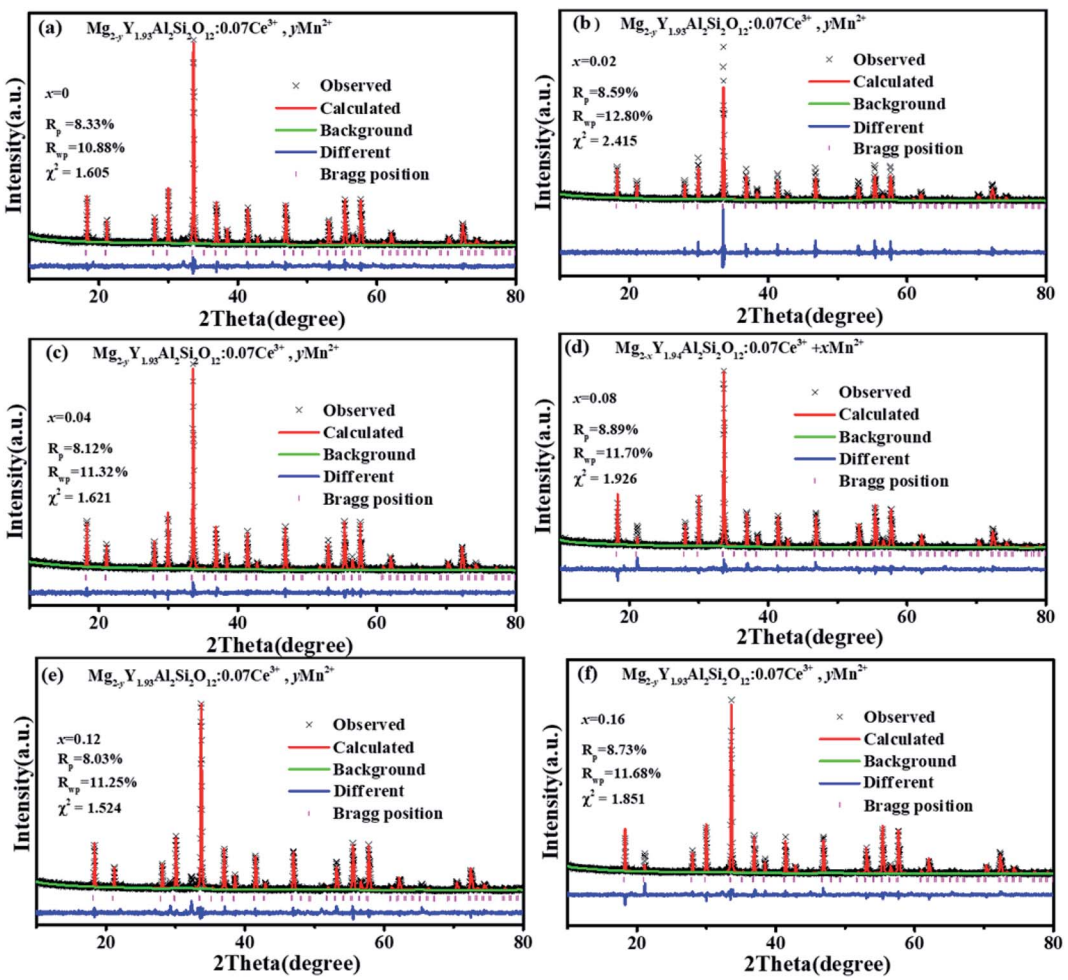

Fig. 3 XRD refinement of $Mg_{2-y}Y_{1.93}Al_2Si_2O_{12}$:0.07 Ce^{3+},yMn^{2+} (y = 0, 0.02, 0.04, 0.12, 0.16).

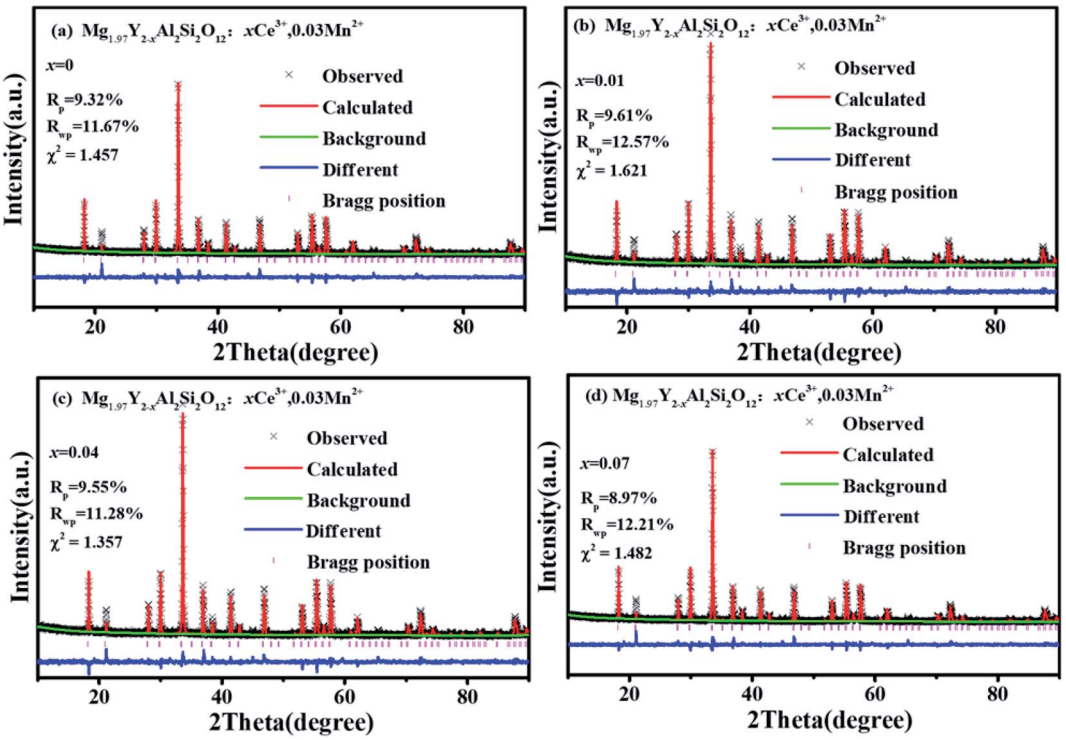

Fig. 4 XRD refinement of $Mg_{1.97}Y_{2-x}Al_2Si_2O_{12}$:$xCe^{3+}$,0.03 Mn^{2+} (x = 0, 0.01, 0.03, 0.07).

located at 405 nm. By monitoring the 405 nm emission peak, the excitation spectrum ranges from 200 to 400 nm, and the strongest excitation peak is 332 nm, which is formed by the electron transition from the ground state to $5d_2$ energy level. The tailing of 500–650 nm comes from the emission spectrum of electrons from $5d_2$ level relaxing to $5d_1$ level and then downward. In Fig. 5(b), under the excitation of 470 nm, it is seen that the emission spectrum extends from 500 nm to 800 nm and the emission peak is at 600 nm. For the 600 nm emission peak, the corresponding excitation spectrum extends from 200 nm to 550 nm. It is obvious that there are two excitation peaks in the excitation spectrum: one is ~332 nm, which is attributed to the electronic transition from the ground state to the $5d_2$ level, and the other one is at 470 nm, which is attributed to the electron transition from the ground state to the $5d_1$ level.

In the previous work, it has been proven that Mn^{2+} ions can occupy the tetracoordinate, hexacoordinate and octagonal sites of $Mg_2Y_2Al_2Si_2O_{12}$ and emit green light (536 nm), red light (635 nm) and deep red light (735 nm). When the amount of Mn^{2+} is > 0.2, the deep red light will be generated. The purpose of this work is to develop a red-light-compensated phosphor; hence, the amount of Mn^{2+} ions is not >0.2. Fig. 5(c) and (d) show the excitation spectra and emission spectra of $Mg_{1.97}Y_2Al_2Si_2O_{12}$:0.03 Mn^{2+}. According to the literature, Mn ions can occupy four, six and eight coordination in garnet structure.[42] In this work, Mn^{2+} occupies eight coordination sites to form the luminescence center Mn1. Under the excitation of 421 nm, the emission spectrum extends from 470 to 700 nm, and the primary peak is located at 635 nm. By monitoring the 635 nm emission peak, the excitation spectrum from 200 nm to 500 nm is obtained, and the peak is at 421 nm. The 536 nm emission peak is derived from the luminescence center Mn2 formed by Mn^{2+} occupying a tetracoordinate position, as shown in Fig. 5(d). For the luminescence center Mn2, the emission spectrum extends from 500 to 750 nm under the 456 nm excitation radiation; furthermore, the peak is at 536 nm. For the 536 nm emission peak, a broad excitation band is observed from 200 nm to 500 nm, and the primary peak is at 456 nm.

Fig. 5 show that the emission spectrum of Ce^{3+} overlaps with the excitation spectrum of Mn^{2+} in the yellow- and green-shaded region and that the luminescence center formed by Ce^{3+} may transfer energy to the luminescence centers Mn1 and Mn2. Moreover, the emission peak of Mn^{2+} ion is closer to the long-wave direction; furthermore, the red component of $Mg_2Y_{1.93}Al_2Si_2O_{12}$:0.07 Ce^{3+} can be enhanced by co-doping Mn^{2+}. In addition, under the same measurement conditions, the ratio of the relative emission intensity of Ce^{3+} to Mn^{2+} is ~100 : 1.

3.3 Luminescence properties of $Mg_{1.97}Y_{1.93}Al_2Si_2O_{12}$:0.07 Ce^{3+},0.03 Mn^{2+}

Fig. 6(a) shows the emission spectrum of $Mg_{1.97}Y_{1.93}Al_2Si_2O_{12}$:0.07 Ce^{3+},0.03 Mn^{2+} under the 470 nm excitation and the primary peak is at 618 nm. Compared with the emission peak of $Mg_2Y_{1.93}Al_2Si_2O_{12}$:0.07 Ce^{3+} is at 600 nm in Fig. 5(b), the emission spectrum of $Mg_{1.97}Y_{1.93}Al_2Si_2O_{12}$:0.07 Ce^{3+},0.03 Mn^{2+} results in a significant redshift. No characteristic emission spectrum of Mn^{2+} is observed in the spectrum, and the characteristic excitation of Mn^{2+} ions could not be observed by monitoring the emission peaks of 635 (Mn1) and 536 nm (Mn2).

It may be because the luminescence intensity of Mn^{2+} is considerably smaller than the luminescence intensity of Ce^{3+}. To avoid this interference, the emission spectrum of the sample $Mg_{1.97}Y_{1.93}Al_2Si_2O_{12}$:0.07 Ce^{3+},0.03 Mn^{2+} is measured under the excitation of 332 nm. Fig. 6(b) shows the 635 nm characteristic emission of Mn1 with the 332 nm excitation, which indicates that Mn^{2+} can normally emit. To further confirm that Mn^{2+} ions form luminescence centers in $Mg_{1.97}Y_{1.93}Al_2Si_2O_{12}$:0.07 Ce^{3+},0.03 Mn^{2+}, the lifetimes of Mn1 and Mn2 are measured; furthermore, the lifetimes can be calculated using the following formula[28–30]

$$\tau = \frac{\int_0^\infty I(t)\mathrm{d}t}{\int_0^\infty I(t)\mathrm{d}t} \quad (1)$$

I refers to the emission intensity of the illuminating center at time t, t is time, and τ is the lifetime. The calculated lifetimes of Mn1 and Mn2 are 3.63 and 0.97 ms, respectively, as shown in Fig. 6(c). It is confirmed that Mn^{2+} ions do form the luminescent centers in the sample and that the emission spectra of the sample $Mg_{1.97}Y_{1.93}Al_2Si_2O_{12}$:0.07 Ce^{3+},0.03 Mn^{2+} is attributed to the interaction of Ce^{3+} and Mn^{2+} luminescence centers.

Fig. 7(a) shows the emission spectra of $Mg_{2-y}Y_{1.93}Al_2Si_2O_{12}$:0.07 Ce^{3+},yMn^{2+} under 470 nm excitation. There is an obvious red shift, which can be observed with Mn^{2+} concentration increased, and the emission peaks of $Mg_{2-y}Y_{1.93}Al_2Si_2O_{12}$:0.07 Ce^{3+},yMn^{2+} shifting from 600 to 635 nm, as shown in Fig. 7(b). The reasons may be explained below:

(1) When doped with Mn^{2+} ions, the crystal structure of the sample changes, resulting in a change in the emission spectra of Ce^{3+}, which causes the redshift of the emission spectra.

(2) Ce^{3+} ions transfer energy to the luminescence center of Mn1, and the emission intensity of Mn1 increases, which causes the emission spectra to move toward the long-wave direction.

For specific reasons, the following experiments were performed.

3.4 Analyze the conjecture (1)

Under the 470 nm excitation, the emission spectrum of Mn1 is indistinguishable from the large-area overlap of the emission spectrum of the Ce^{3+} $5d_1$ level. To reduce the effect of the emission spectrum of the $5d_1$ level, the emission spectra of the samples were measured under 332 nm excitation. Fig. 8(a) shows that the emission peak of the right emission spectrum is at 635 nm, which is attributed to the luminescence center Mn1. As the doping concentration of Mn^{2+} increases, the crystal structure may change; furthermore, the emission spectrum of Mn1 shifts to the long-wave direction. Because Ce^{3+} and Mn1 occupy the same position, the emission spectrum of Ce^{3+} may move in the longwave direction with increase in Mn^{2+} doping concentration. Furthermore, verifying the above conclusions from the perspective of the crystal structure. Many factors describe the change in the crystal field; however, the most influential two factors are the average bond length of the polyhedral unit cell and the degree of distortion of the unit cell. The relationship between the average bond length and the splitting of the luminescent center level orbit can be calculated using the following formula[31]

$$\varepsilon_{\mathrm{cfs}} = \beta_{\mathrm{poly}} R^{-2} \quad (2)$$

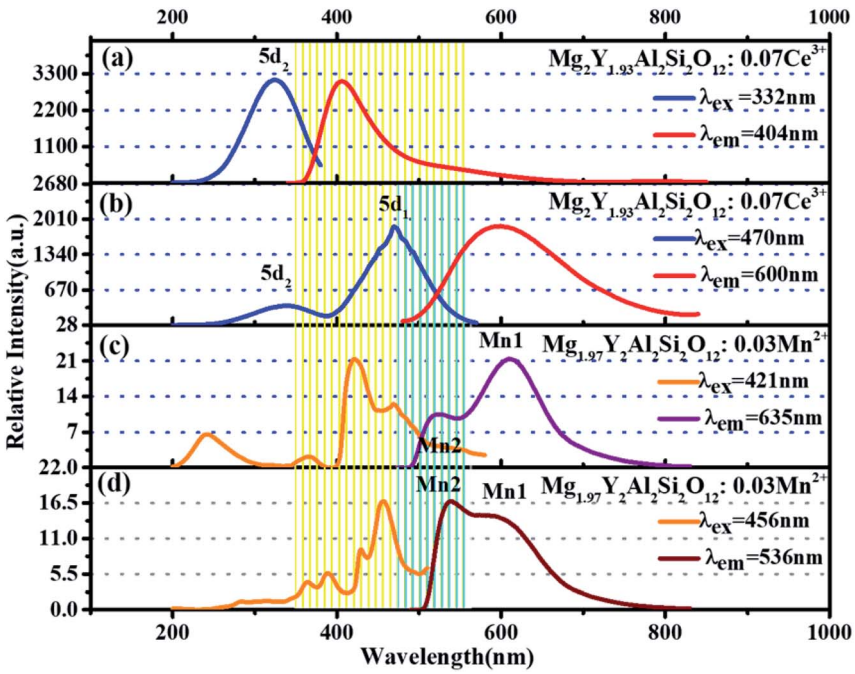

Fig. 5 (a and b) Excitation spectra and emission spectra of $Mg_2Y_{1.93}Al_2Si_2O_{12}$:0.07 Ce^{3+}. (c and d) Excitation spectra and emission spectra of $Mg_{1.97}Y_2Al_2Si_2O_{12}$:0.03 Mn^{2+}.

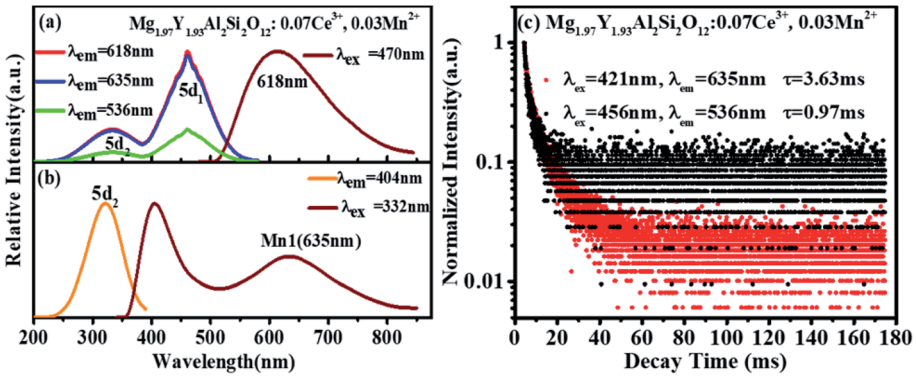

Fig. 6 (a and b) Excitation spectra and emission spectra $Mg_{1.97}Y_{1.93}Al_2Si_2O_{12}$:0.07 Ce^{3+},0.03 Mn^{2+}; (c) lifetime decay spectra of Mn1 and Mn2 in $Mg_{1.97}Y_{1.93}Al_2Si_2O_{12}$:0.07 Ce^{3+},0.03 Mn^{2+}.

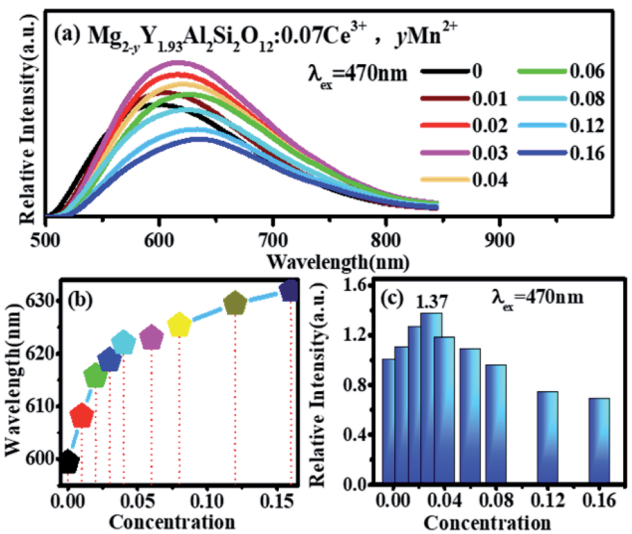

Fig. 7 (a) Emission spectra of $Mg_{2-y}Y_{1.93}Al_2Si_2O_{12}$:0.07 Ce^{3+},yMn^{2+} (y = 0, 0.01, 0.02, 0.03, 0.04, 0.06, 0.08, 0.12, 0.16) (λ_{ex} = 470 nm). (b) A shift diagram of the emission peaks of $Mg_{2-y}Y_{1.93}Al_2Si_2O_{12}$:0.07 Ce^{3+},yMn^{2+} (y = 0, 0.01, 0.02, 0.03, 0.04, 0.06, 0.08, 0.12, 0.16) (λ_{ex} = 470 nm). (c) A change in emission intensity of $Mg_{2-y}Y_{1.93}Al_2Si_2O_{12}$:0.07 Ce^{3+},yMn^{2+} (y = 0, 0.01, 0.02, 0.03, 0.04, 0.06, 0.08, 0.12, 0.16) (λ_{ex} = 470 nm).

ε_{cfs} is the crystal field splitting and β_{poly} is a constant, which depends on the type of polyhedron; generally, $\beta_{octa} = 1.35 \times 10^9$ pm^2 cm^{-1} (octahedron). The β_{poly} of other polyhedral cells can be derived from the octahedral β_{octa}. $\beta_{cub} = 0.89\beta_{octa}$ (cube), $\beta_{dh} = 0.79\beta_{octa}$ (dodecahedron). R^{-2} is the average bond length; therefore, the degree of the orbital splitting of the activated ions increases as R decreases.

As for the crystal distortion, the change in the bond length and bond angle in the crystal can cause the symmetry of the crystal decreasing and lead to the crystal field to split. Conversely, the symmetry of crystal increasing indicates the distortion degree of the crystal decreasing, which reduces the split in the crystal field. It can be calculated using the formula (3),[32,33] and the degree of distortion is affected by the bond length

$$\text{Key length}: D = \frac{1}{n}\sum_{i=1}^{n}\frac{|l_i - l_{av}|}{l_{av}} \quad (3)$$

where l_i represents the bond length of the central atom and the ligand, l_{av} represents the average bond length, and n represents the coordination number. Table 1 shows the XRD refinement data of $Mg_{2-y}Y_{1.93}Al_2Si_2O_{12}$:0.07 Ce^{3+},yMn^{2+} (y = 0, 0.02, 0.04, 0.08, 0.12, 0.16) and the calculated distance between Ce^{3+} ions. The energy level splitting and distortion of $Mg_{2-y}Y_{1.93}Al_2Si_2O_{12}$:0.07 Ce^{3+},yMn^{2+} (y = 0, 0.02, 0.04, 0.08, 0.12, 0.16) was

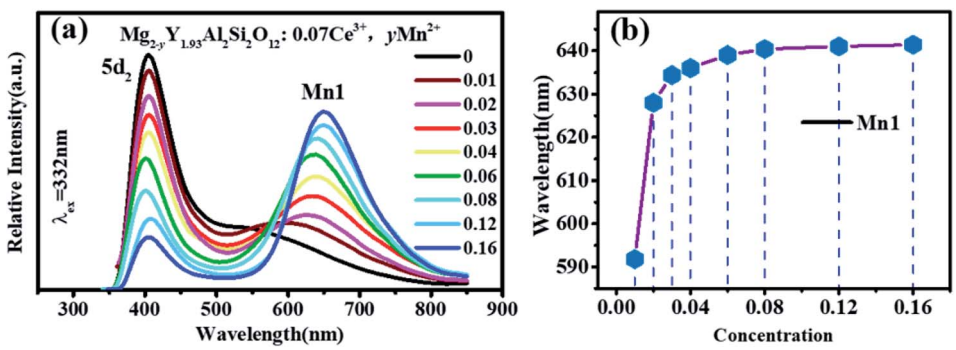

Fig. 8 (a) The emission spectra of the samples $Mg_{2-y}Y_{1.93}Al_2Si_2O_{12}$:0.07 Ce^{3+},yMn^{2+} (y = 0, 0.01, 0.02, 0.03, 0.04, 0.06, 0.08, 0.12, 0.16) at 332 nm excitation; (b) the emission peak shifts of the Mn1 emission spectra.

Table 1 XRD refinement data of $Mg_{2-y}Y_{1.93}Al_2Si_2O_{12}$:0.07 Ce^{3+},yMn^{2+} (y = 0, 0.02, 0.04, 0.08, 0.12, 0.16) and the calculated distance between Ce^{3+} ions

x	0	0.02	0.04	0.08	0.12	0.16
χ^2	1.605	2.415	1.621	1.926	1.524	1.851
R_{wp}	10.88%	12.8%	11.32%	11.7%	11.25%	11.68%
R_p	8.3%	8.59%	8.12%	8.89%	8.03%	8.73%
$a/b/c$ (Å)	11.990	11.992	11.993	11.994	11.995	11.997
V (Å^3)	1723.665	1724.339	1724.819	1725.282	1725.900	1726.763
Eight-coordinated bond lengths m (Å)	2.313	2.313	2.315	2.317	2.319	2.321
Eight-coordinated bond lengths n (Å)	2.4265	2.428	2.431	2.435	2.439	2.443

calculated and the data is shown in Table 2. The crystal field splitting decreases with an increase in the Mn^{2+} concentration; however, at the same time, the unit cell distortion gradually increases, which causes the energy level splitting to increase. In fact, the crystal distortion in the dodecahedral structure of the garnet has a stronger influence on the luminescence center, which makes the emission spectrum shift toward the long-wave direction. The above analyses indicate that speculation (1) is correct. When doped with Mn^{2+} ions, the crystal structure of the sample changes, resulting in the emission redshift of Ce^{3+} and Mn^{2+}.

3.5 Analyze the conjecture (2)

It can be clearly seen from Fig. 8(a) that the Ce^{3+} ions transfer energy to Mn1 under excitation at 332 nm. However, under excitation at 470 nm, the emission spectra of Mn1 cannot be distinguished from the $5d_1$ emission spectra of Ce^{3+}. To confirm that there is an energy transfer between the $5d_1$ emission spectra of Ce^{3+} and the emission spectra of Mn1; the lifetime changes of Ce^{3+} and Mn^{2+} luminescent centers were measured. The lifetimes of Mn1, Mn2, the electron of $5d_1$ and $5d_2$ (using 320 nm and 455 nm external LED pulse lamps) level in $Mg_{1.97}Y_{2-x}Al_2Si_2O_{12}$:$x$$Ce^{3+}$,0.03 Mn^{2+} and $Mg_{2-y}Y_{1.93}Al_2Si_2O_{12}$:0.07 Ce^{3+},yMn^{2+} were measured with an increase in the Mn^{2+} concentration. Fig. 9(a) shows the lifetimes of the luminescence center Mn1. The results show that the lifetimes of the luminescence center Mn1 gradually increases with increase in Ce^{3+} concentration.

Fig. 5 shows that the emission spectrum of Mn2 overlaps with the excitation and emission spectra of Ce^{3+} ions, indicating that the photon energy emitted by the two is close. Therefore, Mn2 may transfer energy to Ce^{3+} ions, and Ce^{3+} may transfer energy to Mn2. The experiment verified the relevant information, and a large number of studies reported that Ce^{3+} transfers energy to Mn^{2+} and examples of Mn^{2+} ion transferring energy to Ce^{3+} have not been found.[34–39] Furthermore, the experiment measured the lifetime change of Mn2 luminescence center with Ce^{3+} doping, as shown in Fig. 9(b). With increase in Ce^{3+} ion doping concentration, the lifetime of Mn2 luminescence center has a slight increase, indicating that Ce^{3+} is in the material and it is possible to transfer energy to Mn2.

Fig. 9 (c–f) show the lifetimes of the $5d_1$ and $5d_2$ level electrons of Ce^{3+} in $Mg_{2-y}Y_{1.93}Al_2Si_2O_{12}$:0.07 Ce^{3+},yMn^{2+}. When the Mn^{2+} concentration is increased, the lifetimes of Ce^{3+} decrease overall (the abnormality of lifetimes is explained in detail below). Consequently, Ce^{3+} ions transfer energy to Mn^{2+} ions, and the emission intensity of Mn1 increases, which causes the emission spectra of the samples $Mg_{2-y}Y_{1.93}Al_2Si_2O_{12}$:0.07 Ce^{3+},yMn^{2+} to move toward the long-wave direction.

Therefore, the primary reasons for the spectral shift are as follows: (1) as the Mn^{2+} ion concentration increases, the distortion of the dodecahedral unit cell increases such that the $5d_1$ level of Ce^{3+} splitting and the crystal field splitting of Mn1 luminescence center increase, the emission spectra move toward the direction of long waves. (2) The Ce^{3+} luminescence center transferred energy to the Mn1 luminescence center, and the luminescence intensity of Mn1 increases, which causes the emission spectra to move toward the long-wave direction. Under the combined action of the two, the emission spectra move toward the long-wave direction as the Mn^{2+} concentration increases.

Moreover, as shown in Fig. 8(a) and 6(a), the energy transfer of Ce^{3+} to Mn1 is more efficient than the Mn2 luminescence center, which indicated that Ce^{3+} has little effect on the luminescence properties of Mn2. This may be attributed to Mn2 being located at the center of the fully symmetric tetrahedron, which greatly weakens the influence of external Mn2 luminescence center. Conversely, it can be considered that the effect of Mn2 on the overall luminescent property of $Mg_{2-y}Y_{1.93}Al_2Si_2O_{12}$:0.07 Ce^{3+},yMn^{2+} is weak.

In Fig. 7(a) and (c), under the excitation of 470 nm, the emission intensities of $Mg_{2-y}Y_{1.93}Al_2Si_2O_{12}$:0.07 Ce^{3+},yMn^{2+} abnormally increases with increase in Mn^{2+} concentration. In Fig. 5, under the same test conditions (photomultiplier voltage is 460 V, excitation end slit width is 2.5 nm, and receiving end slit width is 2.5 nm), the relative emission intensity of Mn^{2+} is

Table 2 The energy level splitting and distortion of $Mg_{2-y}Y_{1.93}Al_2Si_2O_{12}$:0.07 Ce^{3+},yMn^{2+} (y = 0, 0.02, 0.04, 0.08, 0.12, 0.16)

Concentration	Energy level splitting ε_{cfs} (10^9 pm^2 cm^{-1})	Distortion D
0	0.1899	0.0239
0.02	0.1898	0.0243
0.04	0.1894	0.0244
0.08	0.1889	0.0248
0.12	0.1885	0.0253
0.16	0.1880	0.0255

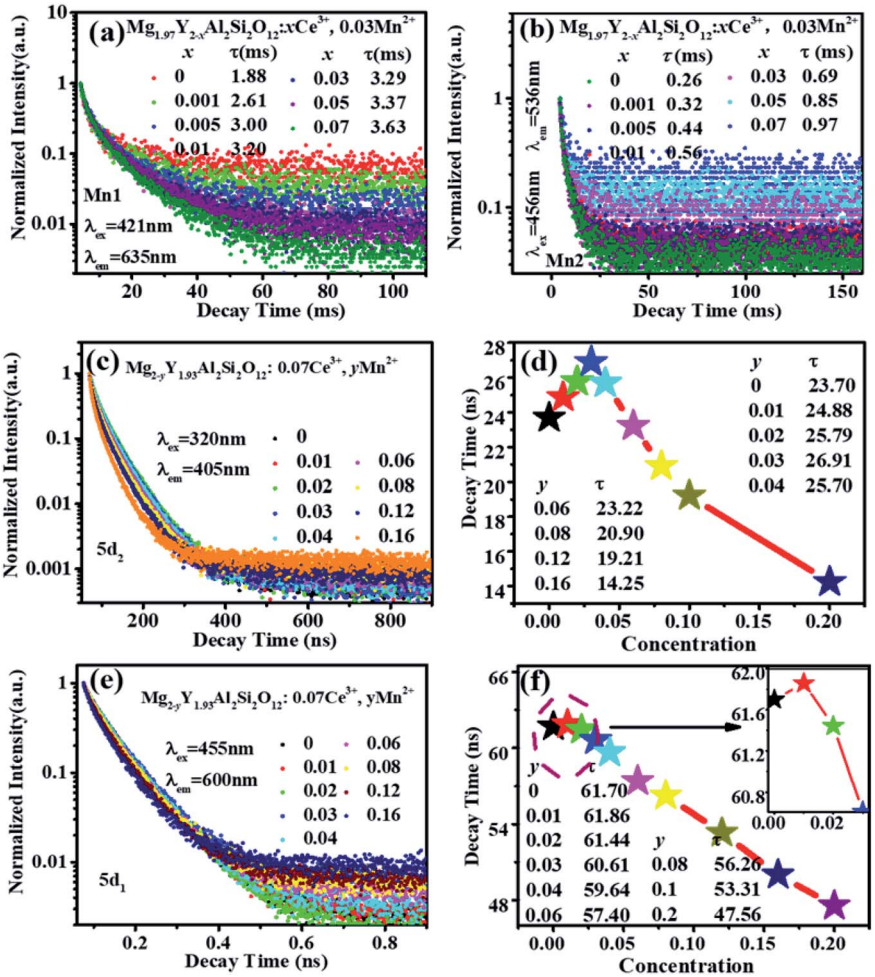

Fig. 9 (a) Lifetimes of Mn1 luminescence center in $Mg_{1.97}Y_{2-x}Al_2Si_2O_{12}$:$xCe^{3+}$,0.03 Mn^{2+} (λ_{ex} = 421 nm, λ_{em} = 635 nm); (b) the lifetimes of Mn2 luminescence center in $Mg_{1.97}Y_{2-x}Al_2Si_2O_{12}$:$xCe^{3+}$,0.03 Mn^{2+} (λ_{ex} = 456 nm, λ_{em} = 536 nm); (c and d) the lifetimes of the $5d_2$ level electrons of Ce^{3+} in $Mg_{2-y}Y_{1.93}Al_2Si_2O_{12}$:0.07 Ce^{3+},yMn^{2+} and the corresponding line graph (λ_{ex} = 320 nm, λ_{em} = 405 nm); (e and f) the lifetime of the $5d_1$ level of Ce^{3+} in $Mg_{2-y}Y_{1.93}Al_2Si_2O_{12}$:0.07 Ce^{3+},yMn^{2+} and the corresponding line graph (λ_{ex} = 455 nm, λ_{em} = 600 nm).

much smaller than that of Ce^{3+}. The emission intensities of Mn^{2+} are negligible compared to the overall Ce^{3+} emission spectra. Though Ce^{3+} can transfer energy to the Mn1 luminescence center, the energy utilization efficiency must be generally <100%, which will lose energy. Namely, the number of photons absorbed by the Mn1 luminescence center will be higher than the number of photons radiated. If there are no other factors, as the Mn^{2+} concentration increases, the transfer energy increases and the energy loss increases under the 470 nm excitation; therefore, the overall emission intensity of the sample should

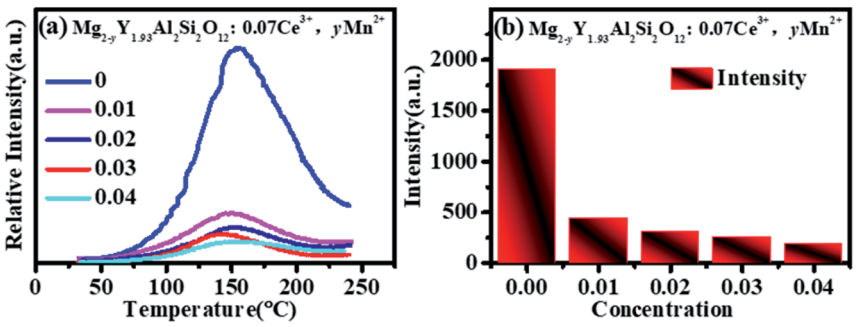

Fig. 10 (a) Thermoluminescence spectra of $Mg_{2-y}Y_{1.93}Al_2Si_2O_{12}$:0.07 Ce^{3+},yMn^{2+} (y = 0, 0.01, 0.02, 0.03, 0.04). (b) The thermoluminescence intensity of $Mg_{2-y}Y_{1.93}Al_2Si_2O_{12}$:0.07 Ce^{3+},yMn^{2+} as a function of Mn^{2+} concentration.

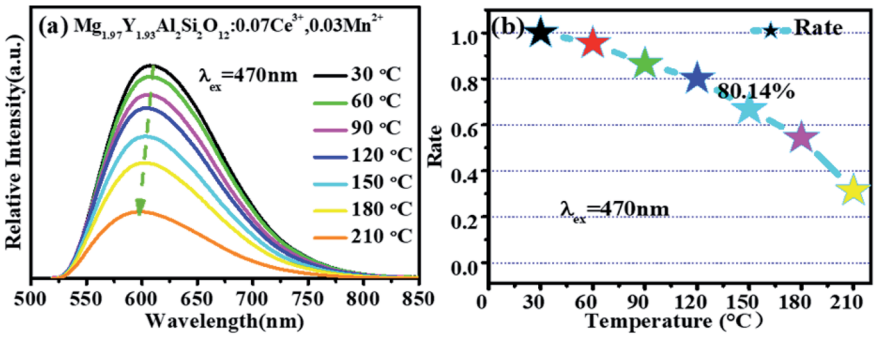

Fig. 11 (a) Temperature spectra of $Mg_{1.97}Y_{1.93}Al_2Si_2O_{12}$:0.07 Ce^{3+},0.03 Mn^{2+}. (b) The emission intensity of $Mg_{1.97}Y_{1.93}Al_2Si_2O_{12}$:0.07 Ce^{3+},0.03 Mn^{2+} as a function of temperature.

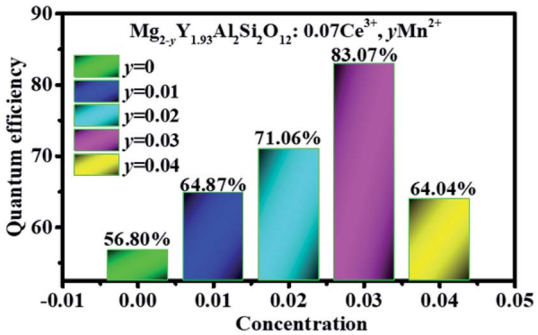

Fig. 12 Quantum efficiency of $Mg_{2-y}Y_{1.93}Al_2Si_2O_{12}$:0.07 Ce^{3+},yMn^{2+} (y = 0, 0.01, 0.02, 0.03, 0.04).

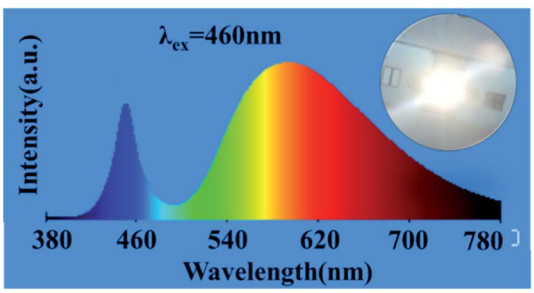

Fig. 13 Mixed phosphor of YAG:Ce^{3+} and $Mg_{1.97}Y_{1.93}Al_2Si_2O_{12}$:0.07 Ce^{3+},0.03 Mn^{2+} is excited by the 460 nm chip.

gradually decrease. However, it is observed that the emission intensities of the samples abnormally increase under the 470 nm excitation with an increase in the Mn^{2+} concentration and reach a maximum at 0.03, as shown in Fig. 7(c). It can be inferred that other factors cause an abnormal increase in the luminescence intensity of samples under the same excitation radiation. The luminescence centers in the sample are only Ce^{3+} and Mn^{2+}; hence, the possibilities causing the enhanced abnormal luminescence intensity of $Mg_{2-y}Y_{1.93}Al_2Si_2O_{12}$:0.07 Ce^{3+},yMn^{2+} are as follows:

(1) The luminescence intensity of the Mn^{2+} luminescence center itself (excluding the energy transfer of Ce^{3+}) in the $Mg_{2-y}Y_{1.93}Al_2Si_2O_{12}$:0.07 Ce^{3+},yMn^{2+} is considerably improved compared to luminescence intensity in the $Mg_{2-y}Y_2Al_2Si_2O_{12}$:-y$Mn^{2+}$. Thus, the emission intensity of co-doping of Ce^{3+} and Mn^{2+} is higher than that of single-doped Ce^{3+} ions under 470 nm excitation.

(2) Mn^{2+} doping into $Mg_2Y_{1.93}Al_2Si_2O_{12}$:0.07 Ce^{3+} increases the emission intensity of Ce^{3+} ions itself, which improves the overall luminescence intensity.

Next, it will be proved and explained one by one. Fig. 6 shows that the characteristic excitation and emission of Mn1 and Mn2 cannot be observed under excitation of 470 nm when co-doped with Ce^{3+} and Mn^{2+}, which indicates that the luminescence efficiency of Mn^{2+} is relatively weak. Therefore, reasons (1) and (3) are excluded. As such, the reason for the abnormal enhancement of the emission of the sample may be the conjecture (2): Mn^{2+} ions doping into $Mg_2Y_{1.93}Al_2Si_2O_{12}$:0.07 Ce^{3+} increase the emission intensity of Ce^{3+} ions, which improves the overall luminescence intensity. The details of the energy loss between Ce^{3+} ions can be described as Ce^{3+} acts as an active ion in the host because the activated ions at the same excited states are close enough with increasing activator concentration, which can easily result in energy transfer among the energy states. Due to the energy transfer between activator and activator, the energy will go through the quenching center of impurity and be consumed in the lattice vibration of the host, which can further result in a decrease in the emission intensity. In addition, the activating Ce^{3+} ions and defects in the matrix can be used as quenching centers.

Therefore, three factors can improve the emission intensity of Ce^{3+} ions: other ions transfer energy to Ce^{3+}; or the energy loss of Ce^{3+} decreases the quenching center, or Ce^{3+} transferred energy to other luminescent centers decreases. The change of the Ce^{3+} lifetimes can reflect the energy change of the Ce^{3+} luminescence center. This work analyzes the lifetime change of Ce^{3+} ions to determine which factor affects the energy change of the Ce^{3+} luminescence center. This relationship can be expressed by the following formula[40]

$$\frac{1}{\tau} = \frac{1}{\tau_0} + P_{nr} + P_t \quad (4)$$

where τ represents the lifetime of the luminescent center, τ_0 describes the lifetime of the free ion of the luminescent center and is constant. P_{nr} represents the probability of a non-radiative

transition of the luminescent center under the action of the quenching center (negative), and P_t means the probability that the illuminating center absorbs (positively) or outward (negatively). In Fig. 9(d) and (f), the lifetimes of the $5d_1$ and $5d_2$ level electrons of Ce^{3+} in the sample $Mg_{2-y}Y_{1.93}Al_2Si_2O_{12}$:0.07 Ce^{3+},yMn^{2+} increase at first, reaching the maximum at $y = 0.03$, and then gradually decrease. No luminescence centers can transfer energy to Ce^{3+}, and Ce^{3+} ions also transfer energy to Mn^{2+} ions, so P_t is negative. As the Mn^{2+} concentration increases, the P_t value decreases. When doped with a small number of Mn^{2+} ions, the lifetime of Ce^{3+} increases, which proves that there is a certain factor that makes the P_{nr} to increase, namely, the energy loss of the Ce^{3+} ion in the quenching center to decrease. The quenching center of Ce^{3+} can be the other Ce^{3+} ions surrounding the Ce^{3+} luminescence center or the quenching center composed of defects in the matrix structure. So, the reasons for the reduction in energy loss of the corresponding Ce^{3+} luminescence center are as the Mn^{2+} concentration increases, the distance between Ce^{3+} ions increase, which weakens the multipole interaction between Ce^{3+} ions; Mn^{2+} ions reduce the concentration of defects, the number of Ce^{3+} quenching centers and the energy loss of the Ce^{3+} luminescence center. Using the volume of the sample unit cell in Table 1, the distances between the Ce^{3+} ions were calculated using the formula for the critical distance between ions[41]

$$R_c \approx 2\left(\frac{3V}{4\pi\chi_c N}\right)^{\frac{1}{3}} \quad (5)$$

where R_c is the distance between the doped particles, V is the unit cell volume, χ_c is the doping ion concentration, and N is the number of cations in the unit cell. $\chi_c = 0.06$, $N = 8$, and the volume is obtained by refinement data, as shown in Table 1. The distances between Ce^{3+} ions are calculated to be 9.0299, 9.0300, 9.0302, 9.0305, 9.0308, 9.0311, which correspond to $x = 0$, 0.02, 0.04, 0.08, 0.12, 0.16, respectively. The distances between Ce^{3+} ions gradually increase, which means that the interaction probability between Ce^{3+} ions decrease, and the energy loss of the Ce^{3+} luminescence center is reduced.

The thermoluminescence intensity is used to characterize the number of defects in $Mg_{2-y}Y_{1.93}Al_2Si_2O_{12}$:0.07 Ce^{3+},yMn^{2+} (y = 0, 0.01, 0.02, 0.03, 0.04), as shown in Fig. 10. It can be seen that as the Mn^{2+} ions are doped into the material, the number of defects in the sample gradually decreases. Meanwhile, the defect-quenching center number of the Ce^{3+} may be decreasing, which reduces the energy loss of the Ce^{3+} luminescent center. Briefly, with doping of Mn^{2+} ions, the distance between Ce^{3+} particles increase, the interaction between Ce^{3+} particles decrease, the quenching center of defect formation decreases, and the energy loss of Ce^{3+} luminescence center decreases. At low concentration, the energy saved by the quenching center is more than the energy lost by the energy transfer, so that the emission intensities increase. Otherwise, when the doping concentration is relatively high, the energy saved by the quenching center is less than the energy lost by the energy transfer, hence the emission intensity decreases.

3.6 Temperature stability and quantum efficiency

Fig. 11 shows that the emission intensity of $Mg_{1.97}Y_{1.93}Al_2Si_2O_{12}$:0.07 Ce^{3+},0.03 Mn^{2+} gradually decreases with an increase in the temperature, under the excitation of 470 nm light. The emission spectrum intensity remains 80.14% at 120 °C, which means that it has a higher temperature stability.

Fig. 12 shows the quantum efficiency of $Mg_{2-y}Y_{1.93}Al_2Si_2O_{12}$:0.07 Ce^{3+},yMn^{2+} (y = 0, 0.01, 0.02, 0.03, 0.04). Under the 470 nm excitation, the quantum efficiencies of the samples $Mg_{2-y}Y_{1.93}Al_2Si_2O_{12}$:0.07 Ce^{3+},yMn^{2+} increase at first and then decreases with increasing Mn^{2+} concentration, which is the same as the changing trend of the emission spectra. When doped with 0.03 Mn^{2+}, the internal quantum efficiency is as high as 83.07%, which reaches the level of commercial application.

To verify that $Mg_{1.97}Y_{1.93}Al_2Si_2O_{12}$:0.07 Ce^{3+},0.03 Mn^{2+} phosphor can supplement the red component of blue-chip + YAG:Ce^{3+}, the mixed phosphor of YAG:Ce^{3+} and $Mg_{1.97}Y_{1.93}Al_2Si_2O_{12}$:0.07 Ce^{3+},0.03 Mn^{2+} was excited by the 460 nm chip, and a warm white LED with the color temperature of 3005 K was successfully obtained, as shown in Fig. 13. Moreover, the color rendering index was raised to 78, and the effect of adding red components was remarkable.

4 Conclusions

A series of $Mg_2Y_2Al_2Si_2O_{12}$ and $Mg_2Y_2Al_2Si_2O_{12}$ doped with Ce^{3+} and Mn^{2+} were synthesized by the high-temperature solid-phase method. Two phenomena about the emission spectra of the samples $Mg_{2-y}Y_{1.93}Al_2Si_2O_{12}$:0.07 Ce^{3+},yMn^{2+} are emphatically discussed. The one phenomenon is that the emission spectra are shifted from 600 nm to 635 nm under the excitation of 470 nm, wherein, two reasons are causing the spectra red-shift. Firstly, as the Mn^{2+} ions enter the crystal structure, the energy transfer from the Ce^{3+} ion to the Mn1, the emission intensity of Ce^{3+} decreases and the emission intensity of Mn1 increases, so the emission peak shift toward the long-wave direction. Secondly, with the entry of Mn^{2+} ions, crystal distortion of the dodecahedral unit cells of Ce^{3+} and Mn^{2+} increases, which leads to the energy level split of the Ce^{3+} and Mn1 luminescence center increasing, and the emission spectra shift toward the long wave. Another phenomenon is that the emission spectrum intensity of the sample $Mg_2Y_2Al_2Si_2O_{12}$:Ce^{3+},Mn^{2+} anomalously increased by about 37%, compared with the emission spectrum intensity of the sample $Mg_2Y_2Al_2Si_2O_{12}$:Ce^{3+}, which is because that doping of Mn^{2+} ions increases the distance between the Ce^{3+} ions, and that lowers the concentration of defects in the crystal, resulting in the reduction in the energy loss of the Ce^{3+} quenching center. When the doping concentration of Mn^{2+} is 0.03, the emission peak of the sample $Mg_{1.97}Y_{1.93}Al_2Si_2O_{12}$:0.07 Ce^{3+},0.03 Mn^{2+} shifts to 618 nm and the quantum efficiency was as high as 83.07%. In addition, this sample has high thermal stability, while the emission intensity was still at 80.14% at 120 °C. Finally, warm white light with a high color index of 78 was obtained with abundant red light components by mixing this phosphor with YAG:Ce^{3+}, stimulated by a blue light chip. It has great potential in the application of white LEDs.

Conflicts of interest

The authors declare no competing financial interest.

Acknowledgements

The work is supported by the National Natural Science Foundation of China (No. 51672066, 51902080), the Funds for Distinguished Young Scientists of Hebei Province, China (No. A2018201101), the Natural Science Foundation of Hebei Province, China (No. E2019201223), the personnel training project of Hebei Province, China (No. A201902005), and the Local science and technology development fund projects guided by the central government, China (No. 206Z1102G).

References

1 C. Wang, P. Li, Z. Wang, Y. Sun, J. Cheng, Z. Li, M. Tian and Z. Yang, Crystal structure, luminescence properties, energy transfer and thermal properties of a novel color-tunable, white light-emitting phosphor $Ca_{9-x-y}Ce(PO_4)_7$:xEu^{2+},yMn^{2+}, *Phys. Chem. Chem. Phys.*, 2016, **18**(41), 28661–28673.

2 M. Shang, C. Li and J. Lin, How to produce white light in a single-phase host?, *Chem. Soc. Rev.*, 2014, **43**(5), 1372–1386.

3 S. Ye, F. Xiao, Y. Pan, Y. Ma and Q. Zhang, Phosphors in phosphor-converted white light-emitting diodes: Recent advances in materials, techniques and properties, *Mater. Sci. Eng., R*, 2010, **71**(1), 1–34.

4 C. C. Lin and R. S. Liu, Advances in phosphors for light-emitting diodes, *J. Phys. Chem. Lett.*, 2011, **2**(11), 1268–1277.

5 H. R. Chen, C. Cai and Z. W. Zhang, Enhancing the luminescent efficiency of $Y_3Al_5O_{12}$:Ce^{3+} by coating graphitic carbon nitride: toward white light-emitting diodes, *J. Alloys Compd.*, 2019, **801**, 10–18.

6 L. J. Yin, Y. L. Liang and S. H. Zhang, A novel strategy to motivate the luminescence efficiency of a phosphor: drilling nanoholes on the surface, *Chem. Commun.*, 2018, **54**, 3480–3483.

7 Y. Jia, Y. Huang, Y. Zheng, N. Guo, H. Qiao, Q. Zhao, W. Lv and H. You, Color point tuning of $Y_3Al_5O_{12}$:Ce^{3+} phosphor *via* Mn^{2+}–Si^{4+} incorporation for white light generation, *J. Mater. Chem.*, 2012, **22**(30), 15146–15152.

8 H. Liao, M. Zhao and M. S. Molokeev, Learning from a mineral structure toward an ultra-narrow-band blue-emitting silicate phosphor $RbNa_3(Li_3SiO_4)_4$:Eu^{2+}, *Angew. Chem., Int. Ed.*, 2018, **130**(36), 11902–11905.

9 M. Zhao, H. Liao and M. S. Molokee, Emerging ultra-narrow-band cyan-emitting phosphor for white LEDs with enhanced color rendition, *Light: Sci. Appl.*, 2019, **8**, 38.

10 Y. Li, Y. Shi and G. Zhu, A single-component white-emitting $CaSr_2Al_2O_6$:Ce^{3+},Li^{+},Mn^{2+} phosphor *via* energy transfer, *Inorg. Chem.*, 2015, **45**(14), 7668–7675.

11 M. Jiao, Y. Jia and L. Wei, A single-phase white-emitting $Ca_2SrAl_2O_6$:Ce^{3+},Li^{+},Mn^{2+} phosphor with energy transfer for UV-excited WLEDs, *Dalton Trans.*, 2014, **43**, 3202–3209.

12 G. Blasse and A. Bril, A new phosphor for flying-spot cathode-ray tubes for color television: yellow-emitting $Y_3Al_5O_{12}$–Ce^{3+}, *Appl. Phys. Lett.*, 1967, **11**, 53–55.

13 A. A. Setlur, W. J. Heward, M. E. Hannah and U. Happek, Incorporation of Si^{4+}–N^{3-} into Ce^{3+}-doped garnets for warm white LED phosphors, *Chem. Mater.*, 2008, **20**, 6277–6283.

14 X. Wang, G. Zhou, H. Zhang, H. Li, Z. Zhang and Z. Sun, Luminescent properties of yellowish orange $Y_3Al_{5-x}Si_xO_{12-x}N_x$: Ce phosphors and their applications in warm white light-emitting diodes, *J. Alloys Compd.*, 2012, **519**, 149–155.

15 Z. Pan, Y. Xu, Q. Hu, W. Li, H. Zhou and Y. Zheng, Combination cation substitution tuning of yellow-orange emitting phosphor $Mg_2Y_2Al_2Si_2O1_2$:Ce^{3+}, *RSC Adv.*, 2015, **5**(13), 9489–9496.

16 Y. C. Wu, D. Y. Wang, T. M. Chen, *et al*,. A novel tunable green-to yellow-emitting β-YFS:Ce^{3+} phosphor for solid-state lighting, *ACS Appl. Mater. Interfaces*, 2011, **3**(8), 3195–3199.

17 P. Dorenbos, 5d-level energies of Ce^{3+} and the crystalline environment. I. Fluoride compounds, *Phys. Rev. B: Condens. Matter Mater. Phys.*, 2000, **62**(23), 15640.

18 P. Dorenbos, 5d-level energies of Ce^{3+} and the crystalline environment. II. Chloride, bromide, and iodide compounds, *Phys. Rev. B: Condens. Matter Mater. Phys.*, 2000, **62**(23), 15650.

19 P. Dorenbos, 5d-level energies of Ce^{3+} and the crystalline environment. III. Oxides containing ionic complexes, *Phys. Rev. B: Condens. Matter Mater. Phys.*, 2001, **64**(12), 125117.

20 P. Dorenbos, Relating the energy of the [Xe] $5d_1$ configuration of Ce^{3+} in inorganic compounds with anion polarizability and cation electronegativity, *Phys. Rev. B: Condens. Matter Mater. Phys.*, 2002, **65**(23), 235110.

21 P. Dorenbos, Crystal field splitting of lanthanide $4f^{n-1}5d$-levels in inorganic compounds, *J. Alloys Compd.*, 2002, **341**(1–2), 156–159.

22 P. Dorenbos, 5d-level energies of Ce^{3+} and the crystalline environment. IV. Aluminates and "simple" oxides, *J. Lumin.*, 2002, **99**(3), 283–299.

23 Z. Xia and A. Meijerink, Ce^{3+}-Doped garnet phosphors: composition modification, luminescence properties and applications, *Chem. Soc. Rev.*, 2017, **46**, 275.

24 J. Ueda, K. Aishima and S. Tanabe, Temperature and compositional dependence of optical and optoelectronic properties in Ce^{3+}-doped $Y_3Sc_2Al_{3-x}Ga_xO_{12}$ ($x = 0, 1, 2, 3$), *Opt. Mater.*, 2013, **35**, 1952–1957.

25 A. Setlur and A. Srivastava, On the relationship between emission color and Ce^{3+} concentration in garnet phosphors, *Opt. Mater.*, 2007, **29**, 1647–1652.

26 L. Zhang, J. Zhang, X. Zhang, Z. Hao, H. Zhao and Y. Luo, New yellow-emitting nitride phosphor $SrAlSi_4N_7$:Ce^{3+} and important role of excessive AlN in material synthesis, *ACS Appl. Mater. Interfaces*, 2013, **5**, 12839–12846.

27 Y. C. Wu, D. Y. Wang, T. M. Chen, C. S. Lee, K. J. Chen and H. C. Kuo, A novel tunable green-to yellow-emitting β-

YFS:Ce^{3+} phosphor for solid-state lighting, *ACS Appl. Mater. Interfaces*, 2011, **3**, 3195–3199.

28 S. Lee, C. Huang, T. Chan and T. Chen, Crystal structure evolution and luminescence properties of color tunable solid solution phosphors $Ca_{2+x}La_{8-x}(SiO_4)_{6-x}(PO4)_xO_2:Eu^{2+}$, *Dalton Trans.*, 2016, **45**(3), 1007–1015.

29 D. L. Dexter and J. H. Schulman, Theory of concentration quenching in inorganic phosphors, *J. Chem. Phys.*, 1954, **22**(6), 1063–1070.

30 T. Li, P. Li, Z. Wang, S. Xu, Q. Bai and Z. Yang, Structure, luminescence properties and energy transfer of Tb^{3+}–Eu^{3+} co-doped $LiBaB_9O_{15}$ phosphors, *Dalton Trans.*, 2015, **44**(38), 16840–16846.

31 J. Ueda, K. Aishima, S. Nishiura and S. Tanabe, Afterglow luminescence in Ce^{3+}-doped $Y_3Sc_2Ga_3O_{12}$ ceramics, *Appl. Phys. Express*, 2011, **4**, 042602.

32 Y. Luo and Z. Xia, Effect of Al/Ga Substitution on Photoluminescence and Phosphorescence Properties of Garnet-Type $Y_3Sc_2Ga_{3-x}Al_xO_{12}:Ce^{3+}$ Phosphor, *J. Phys. Chem. C*, 2014, **118**, 23297–23305.

33 L. Chen, C. C. Lin, C. W. Ye and R. S. Liu, Light converting inorganic phosphors for white light-emitting diodes, *Materials*, 2010, **3**, 2172–2195.

34 J. Si, L. Wang and L. Liu, Structure, luminescence and energy transfer in Ce^{3+} and Mn^{2+} codoped γ-AlON phosphors, *J. Mater. Chem. C*, 2019, **7**, 733–742.

35 W. Lv, Y. Jia and Q. Zhao, A novel tunable $Na_2Ba_6(Si_2O_7)(SiO_4)_2:Ce^{3+},Mn^{2+}$ phosphor with excellent thermal stability for white light emitting diodes, *RSC Adv.*, 2014, **4**, 14074–14080.

36 Z. Wang, S. Lou and P. Li, Enhanced orange–red emission of $Sr_3La(PO_4)_3:Ce^{3+},Mn^{2+}$ *via* energy transfer, *J. Lumin.*, 2014, **156**, 87–90.

37 K. Li, M. Shang and Y. Zhang, Photoluminescence properties of single-component white-emitting $CaBi(PO_4)_7:Ce^{3+},Tb^{3+},Mn^{2+}$ phosphors for UVLEDs, *J. Mater. Chem. C*, 2015, **3**(27), 7096–7104.

38 N. Guo, Y. Huang and Y. Jia, A novel orange-yellow-emitting $Ba_3Lu(PO_4)_3:Eu^{2+},Mn^{2+}$ phosphor with energy transfer for UV-excited white LEDs, *Dalton Trans.*, 2013, **42**(4), 941–947.

39 Z. Wang, S. Lou and P. Li, Enhanced orange–red emission of $Sr_3La(PO_4)_3:Ce^{3+},Mn^{2+}$ *via* energy transfer, *J. Lumin.*, 2014, **156**, 87–90.

40 G. Blasse, Energy transfer in oxidic phosphors, *Phys. Lett. A*, 1968, **28**(6), 444–445.

41 J. Kacher, C. Landon, B. L. Adams and D. Fullwood, Bragg's law diffraction simulations for electron backscatter diffraction analysis, *Ultramicroscopy*, 2009, **109**(9), 1148–1156.

42 J. A. Hodges, Temperature dependent epr measurements of Mn^{2+} in diamagnetic garnets, *J. Phys. Chem. Solids.*, 1974, **35**(10), 1385–1392.